Lattice Dynamics of Semiconducting, Metallic, and Superconducting $Ba_{1-x}K_xBiO_3$ Studied by Inelastic Neutron Scattering

Mark A. Green

Royal Institution of Great Britain, 21 Albemarle Street, London W1X 4BS, U.K.

Kosmas Prassides

School of Chemistry and Molecular Science, Sussex University, Brighton BN1 9QJ, U.K., and Royal Institution of Great Britain, 21 Albemarle Street, London W1X 4BS, U.K.

D. A. Neumann

Reactor Radiation Division, National Institute of Standards and Technology, Gaithersburg, Maryland 20899

Peter Day

Royal Institution of Great Britain, 21 Albemarle Street, London W1X 4BS, U.K.

Received October 25, 1994. Revised Manuscript Received February 23, 1995[⊗]

Inelastic neutron scattering has been used to study the lattice dynamics in $Ba_{1-x}K_xBiO_3$ over a wide range of compositions, covering regions of the [composition (x), temperature (T)] phase diagram displaying semiconducting, metallic, and superconducting behavior. Modes are assigned using interatomic potentials calculations, which show good agreement with experiment. The oxygen phonon modes are very sensitive to changes in composition and oxidation state of the Bi ions. Phonon anomalies observed in both the oxygen TO bending (~33 meV) and stretching (~62 meV) modes as a function of temperature are discussed within the context of the BCS theory. Novel behavior is shown by the LO oxygen bending mode at ~42 meV that shows a strong dependence on composition, proposed to arise from the occurrence of structural phase transitions in this system.

Introduction

In recent years a diverse array of metallic materials which undergo a transition to a superconducting state has been discovered. In addition to the elemental and alloy materials,[1] many families of layered cuprates, quaternary intermetallic compounds,[2] and alkali-metal fullerides[3] show such a transition. Among the superconducting oxides, $(Ba,K)BiO_3$[4] and $Ba(Pb,Bi)O_3$[5] are of particular interest, as they have simple three-dimensionally connected perovskite structures and relatively high transition temperatures (32 and 13 K, respectively) despite a low density of states at the Fermi level[6] and the absence of magnetic ions.[7] At low temperatures, the parent oxide, $BaBiO_3$, adopts a monoclinic structure ($I2/m$)[8-10] and contains tilted (along the [110] axis) corner-sharing BiO_6 octahedra with alternating short and long Bi–O bonds (2.12 and 2.28 Å), resulting in a charge density wave (CDW) commensurate with the lattice and semiconducting properties. Upon potassium doping, $Ba_{1-x}K_xBiO_3$ shows two structural phase transitions with increasing x. At first, near $x \sim 0.1$, the breathing mode distortion disappears, leading to an orthorhombic structure ($Ibmm$) and identical Bi–O bonds. Then, at $x \sim 0.375$, the octahedral tilt distortion is suppressed, resulting in a metallic cubic perovskite ($Pm\bar{3}m$) system.

The question of the mechanism responsible for superconductivity in the high-T_c materials is still actively pursued. While in conventional alloy and elemental superconductors, phonon-mediated pair binding is well established, the situation in the cuprates is more subtle. For example, measurements of the neutron-weighted phonon density of states (PDOS) show little difference between superconducting $(La,Sr)_2CuO_4$ and its parent

[⊗] Abstract published in *Advance ACS Abstracts,* April 1, 1995.

(1) Etourneau, J. In *Solid State Chemistry: Compounds*; Cheetham, A. K., Day, P., Eds.; Clarendon Press: Oxford, 1992.

(2) Cava, R. J.; Takagi, H.; Zandbergen, H. W.; Krajewski, J. J.; Peck, W. F.; Siegrist, T.; Batlogg, B.; Vandover, R. B.; Felder, R. J.; Mizuhashi, K.; Lee, J. O.; Eisaki, H.; Uchida, S. *Nature* **1994**, *367*, 252.

(3) Hebard, A. F.; Rosseinsky, M. J.; Haddon, R. C.; Murphy, D. W.; Glarum, S. H.; Palstra, T. T. M.; Ramirez, A. P.; Kortan, A. R. *Nature* **1991**, *350*, 600.

(4) Mattheiss, L. F.; Gyorgy, E. M.; Johnson, D. W. *Phys. Rev. B* **1988**, *37*, 3745.

(5) Sleight, A. W.; Gilson, J. L.; Bierstedt, P. E. *Solid State Commun.* **1975**, *17*, 27.

(6) Itoh, T.; Kitazawa, K.; Tanaka, S. *J. Phys. Soc. Jpn.* **1984**, *53*, 2668.

(7) Uemura, Y.; Sternlieb, B. J.; Cox, D. E.; Brewer, J. H.; Kadono, R.; Kempton, J. R.; Keifl, R. F.; Kreitzman, S. R.; Luke, G. M.; Mulhern, P.; Riseman, T.; Williams, D. L.; Kossler, W. J.; Yu, X. H.; Stronach, C. E.; Subramanian, M. A.; Gopalakrishnan, J.; Sleight, A. W. *Nature* **1988**, *335*, 151.

(8) Cox, D. E.; Sleight, A. W. *Acta Crystallogr. B* **1979**, *35*, 1.

(9) Pei, S.; Jorgensen, J. D.; Dabrowski, B.; Hinks, D. G.; Richards, D. R.; Mitchell, A. W.; Newsam, J. M.; Sinha, S. K.; Vaknin, D.; Jacobsen, A. J. *Phys. Rev. B* **1990**, *41*, 4126.

(10) Thornton, G.; Jacobsen, A. J. *Acta Crystallogr. B* **1978**, *34*, 351.

0897-4756/95/2807-0888$09.00/0

La_2CuO_4,[11] or above and below the superconducting transition temperature in $Bi_2Sr_2CaCu_2O_8$ ($T_c \sim 80$ K).[12] Recently, frequency shifts induced by the appearance of the superconducting energy gap have been measured in large homogeneous single crystals of $Bi_2Sr_2CaCu_2O_8$ and $YBa_2Cu_3O_7$ away from the Brillouin zone center,[13,14] supporting some phonon involvement in the pairing mechanism.

$Ba_{1-x}K_xBiO_3$ is an auspicious system to study in this context, as its simple cubic perovskite structure is reflected in a less complicated phonon spectrum. The observation of a large oxygen isotope effect confirms that oxygen phonon modes are involved in the pairing interaction. Loong et al. measured an isotope effect exponent, $\alpha = 0.42$ by inelastic neutron scattering,[15] in good agreement with the values of Hinks et al. ($\alpha = 0.41$) and Kondoh et al. ($\alpha = 0.35$)[16] derived from the change in T_c upon ^{18}O isotopic substitution.[17] In addition, the measured values deviate little from $\alpha = 0.5$, in agreement with the weak coupling limit of the BCS model. Tunneling measurements[18,19] and the subsequent extraction of the electron–phonon coupling function, $\alpha(\omega)$,[20] from molecular dynamic calculations, also point to the involvement of phonons, particularly the high-energy oxygen modes, in the superconductivity in these systems. Previous studies using inelastic neutron scattering (INS) on polycrystalline materials[21–23] have also revealed the softening of oxygen modes on potassium doping of $BaBiO_3$ to give $Ba_{0.6}K_{0.4}BiO_3$. All these are in agreement with the premise of BCS-like behavior in superconducting $Ba_{0.6}K_{0.4}BiO_3$ with weak coupling to high-energy oxygen modes.

In this paper, we present temperature-dependent high-resolution inelastic neutron scattering (INS) data on $Ba_{1-x}K_xBiO_3$ ($0 \le x \le 0.4$) compositions over an extensive range of doping level x, embracing semiconducting, metallic, and superconducting behavior. Evidence is presented of pronounced frequency and lineshape changes as a function of both temperature and composition. Detailed mode assignments are also made on the basis of phonon calculations.

Experimental Procedure

Powder samples of $BaBiO_3$ were made by mixing $Ba(NO_3)_2$ and Bi_2O_3 in stoichiometric quantities, and heating to 850 °C for 2 days in air and at 450 °C for 4 h in O_2, with intermittent regrindings. $Ba_{1-x}K_xBiO_3$ (x = 0.25, 0.30, 0.35, and 0.40) samples were synthesized by mixing $BaBiO_3$, KO_2, and Bi_2O_3 in stoichiometric quantities and following the two-step procedure described by Hinks et al.[24] This was repeated several times to give single-phase, homogeneous materials. X-ray and neutron diffraction, SQUID magnetometry, and conductivity measurements were used to characterize the materials and were consistent with previously published results.

Inelastic neutron scattering measurements were performed on the time-focused crystal analyzer (TFXA) spectrometer at ISIS, Rutherford Appleton Laboratory, U.K., and on the BT4 triple-axis spectrometer at the National Institute of Standards and Technology, Gaithersburg, TN. TFXA is an inverted-geometry instrument, operating at a fixed neutron final energy of $E_f \sim 4$ meV and with initial energy analysis performed by the time-of-flight technique. Time and energy focusing gives excellent resolution, $(\delta\omega/\omega) \sim 1-2\%$, over a wide range of energies. Samples were mounted in aluminum foil and cooled in a closed-cycle helium refrigerator to 22 K. The measurements on the BT4 spectrometer employed 40′–40′ collimation together with a Cu(220) monochromator and a Be filter analyzer ($E_f < 5$ meV). Samples were mounted in aluminum containers and cooled in a closed-cycle helium refrigerator to 10 K. For both sets of measurements, background runs were measured, normalized to the data sets and subtracted. The background-subtracted data were fitted using Gaussian functions to extract accurate width and position parameters.

For both instruments used in the present work, the scattering law, $S(Q,\omega)$, which is related to the phonon density of states in the incoherent approximation[25] can be obtained:

$$S(Q,\omega) = \sum_i \frac{c_i\sigma_i}{m_i}\langle(\mathbf{Q}\cdot\mathbf{e}_i)^2 e^{-W_i(Q)}\rangle \frac{n(\omega)+1}{\omega} F_i(\omega) \qquad (1)$$

where c_i is the concentration, σ_i is the total coherent scattering cross section, m_i is the mass, $\mathbf{e}_i$ is the phonon unit-polarization vector, $W_i(Q)$ is the Debye–Waller factor, $F_i(\omega)$ is the density of states for the ith atom, $\mathbf{Q}$ is the momentum transfer, and $n(\omega)$ is the Bose thermal occupation factor. The angular brackets $\langle\ \rangle$ reflect the averaging over all $\mathbf{Q}$ for all orientations in a polycrystalline sample. For small fixed final energy instruments,[26] the ratio (Q^2/ω) in eq 1 is essentially constant, and the measured scattering law is directly proportional to the generalized phonon density of states, $g(\omega)$:

$$g(\omega) = \sum_i \frac{c_i\sigma_i}{m_i}\langle(\hat{\mathbf{Q}}\cdot\mathbf{e}_i)^2 e^{-W_i}\rangle F_i(\omega) \qquad (2)$$

where $\hat{\mathbf{Q}}$ is a unit vector along $\mathbf{Q}$ and $\langle\ \rangle$ indicates an averaging over $\mathbf{Q}$ space. In a neutron experiment, eq 2 shows that the contribution, $F_i(\omega)$, from each individual ion to the PDOS is weighted by a factor, σ_i/m_i. In the present case, the values of σ_i/m_i are 0.044 for Ba, 0.056 for K, 0.024 for Bi, and 0.265 for O, implying a strong contribution to the total scattering from oxygen modes.

Phonon Calculations

The phonon density of states (PDOS) and the phonon dispersion relations throughout the Brillouin zone were calculated for (Ba,K)BiO_3 with the program GULP.[27] Double Buckingham interatomic potentials derived before from structural information for these systems

(11) Rosseinsky, M. J.; Prassides, K.; Day, P.; Dianoux, A. J. *Phys. Rev. B* **1988**, *37*, 2231.
(12) Renker, B.; Gompf, F.; Gering, E.; Ewert, D.; Rietschel, H.; Dianoux, A. J. *Z. Phys. B* **1988**, *73*, 309.
(13) Mook, H. A.; Chakoumakos, B. C.; Mostoller, M.; Boothroyd, A. T.; Paul, D. M. *Phys. Rev. Lett.* **1992**, *69*, 2272.
(14) Pyka, N.; Reichardt, W.; Pintschovinus, L.; Engel, G.; Rossat-Mignod, J.; Henry, J. Y. *Phys. Rev. Lett.* **1993**, *70*, 1457.
(15) Loong, C.; Hinks, D. G.; Vashishta, P.; Jin, W.; Kalia, R. K.; Degani, M. H.; Price, D. L.; Jorgensen, J. D.; Dabrowski, B.; Mitchell, A. W.; Richard, D. R.; Zheng, Y. *Phys. Rev. Lett.* **1991**, *66*, 3217.
(16) Kondoh, S.; Sera, M.; Ando, Y.; Sato, Y. *Physica C* **1989**, *157*, 469.
(17) Hinks, D. G.; Richards, D. R.; Dabrowski, B.; Marx, D. T.; Mitchell, A. W. *Nature* **1988**, *335*, 419.
(18) Huang, Q.; Zasadzinski, J. F.; Tralshawala, N.; Gray, K. E.; Hinks, D. G.; Peng, J. L.; Greene, R. L. *Nature* **1990**, *347*, 369.
(19) Zasadzinski, J. F.; Tralshawala, N.; Hinks, D. G.; Dabrowski, B.; Mitchell, A. W.; Richards, D. R. *Physica C* **1989**, *158*, 519.
(20) Jin, W.; Degani, M. H.; Kalia, R. K.; Vashista, P. *Phys. Rev. B* **1992**, *45*, 5535.
(21) Prassides, K.; Rosseinsky, M. J.; Dianoux, A. J.; Day, P. *J. Phys. C: Condens. Matter* **1992**, *4*, 965.
(22) Belushkin, A. V.; Vagov, A. V.; Zemlyanov, M. G.; Parshin, P. P. *Physica C* **1992**, *199*, 103.
(23) Loong, C.; Vashishta, P.; Kalia, R. K.; Jin, W.; Degani, M. H.; Hinks, D. G.; Price, D. L.; Jorgensen, J. D.; Dabrowski, B.; Mitchell, A. W.; Richards, D. R.; Zheng, Y. *Phys. Rev. B* **1992**, *45*, 8052.
(24) Hinks, D. G.; Dabrowski, B.; Jorgensen, J. D.; Mitchell, A. W.; Richards, D. R.; Pei, S.; Shi, D. *Nature* **1988**, *333*, 836.
(25) Miceli, P. F.; Youngquist, S. E.; Neumann, D. A.; Zabel, H. *Phys. Rev. B* **1986**, *34*, 8977.
(26) Sumarlin, I. W.; Lynn, J. W.; Neumann, D. A.; Rush, J. J.; Loong, C.-K.; Peng, J. L.; Li, Z. Y. *Phys. Rev. B* **1993**, *48*, 473.
(27) Gale, J. D. Royal Institution of Great Britain and Imperial College, 1992–1994.

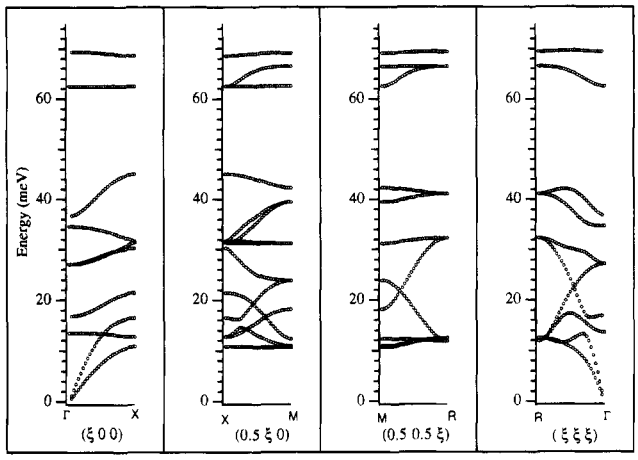

Figure 1. Calculated phonon dispersion curves in cubic (Ba,K)BiO_3.

Table 1. Charges and Spring Constants for Barium, Bismuth, and Oxygen Used in the Interatomic Potential Phonon Calculations

ion	type	charge (e)	spring constant (eV/Å^2)
O^{2-}	core	0.386	18.41
	shell	−2.386	
Ba^{2+}	core	0.152	29.1
	shell	1.848	
Bi^{4+}	core	34	11000
	shell	−30	

were employed.[28] Core-shell spring constants and charges for O^{2-} and Ba^{2+} ions were used as derived for related perovskite oxides[29] (Table 1). Two systems were investigated: a cubic ($Pm\bar{3}m$) perovskite in which the masses of the A-site ions were set equal to $m_A = 0.6m_{Ba} + 0.4m_K$, corresponding to the stoichiometry $Ba_{0.6}K_{0.4}BiO_3$ and a monoclinic ($I2/m$) perovskite of stoichiometry $BaBiO_3$. Figure 1 shows the calculated phonon dispersion curves for the cubic system along some high-symmetry directions in the Brillouin zone (from Γ to M to X to R and back to Γ). Figure 2 shows the calculated PDOS (together with the contributions from each individual atom) for both systems.

In both cases, the PDOS can be divided roughly into four regions. At low energies, the acoustic modes extend between 0 and 15 meV, with a large peak at ~12 meV caused by the small dispersion of the external optical mode (for a detailed description of each type of phonon modes see Uchida et al.[30]), which is almost completely associated with Ba vibrations. The density of states in the 25−32 meV range is principally due to optically inactive phonons; one branch around 32 meV shows very little dispersion, while the other extends down to 12 meV. Both the bending and stretching modes show very little dispersion and are located at 40−45 and 60−70 meV, respectively, with a >10 meV gap between them. They are characterized by large splittings of the longitudinal (LO) and transverse optic (TO) modes, in good agreement with the experimental infrared data of Uchida et al.[30] While there is a broad similarity in the calculated PDOS for the two systems, two differences

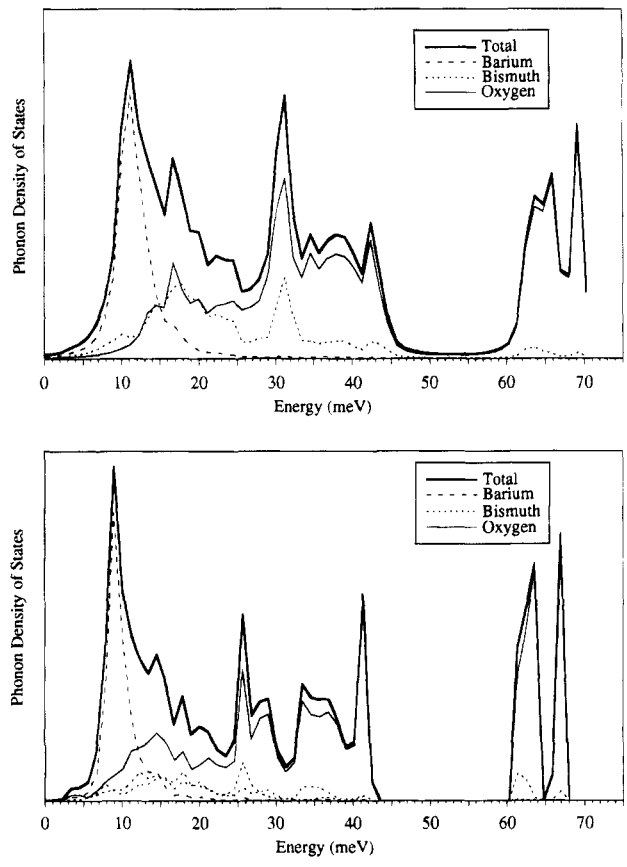

Figure 2. (a, top) Phonon density of states of cubic (Ba,K)BiO_3. (b, bottom) Phonon density of states of monoclinic $BaBiO_3$.

are immediately apparent: the existence of a gap in the PDOS at ~30 meV and the sharpening of the ~42 meV phonon for $BaBiO_3$.

The present phonon calculations are in excellent agreement with optical measurements and with the neutron data presented in this paper, with all phonon modes unambiguously identified (see discussion below).

Results

The neutron-weighted PDOS in $Ba_{1-x}K_xBiO_3$ was measured on TFXA in both the semiconducting (x = 0.25) and the metallic and superconductor composition (x = 0.4) at 22 K. A further measurement was performed on the x = 0.4 compound at 45 K, above the superconducting transition temperature. Figures 3 and 4 show the spectra at 22 K for x = 0.25 and x = 0.4, respectively. For $Ba_{0.75}K_{0.25}BiO_3$, the results of fitting each peak with Gaussians are tabulated in Table 2. The data below 10 meV were excluded from the analysis due to poor instrumental resolution. Structure is resolvable in the spectra up to 75 meV. The peaks at 11.1, 13.2, and 16.1 meV should correspond to the complicated splitting in the TO external mode, and together with the possibility of some acoustic mode contribution, make definite mode assignment difficult; however, the eigenvectors are mostly of Ba character. The broad peak centered around 14.9 meV is mostly of acoustic mode character, containing contributions from both Ba and Bi atoms. The relatively sharp peak at 22.2 meV can be tentitively assigned to the LO external mode, as it is quite distinct from the group of modes below in energy and remains unchanged throughout the range of com-

(28) Zhang, X.; Catlow, C. R. A. *Physica C* **1991**, *173*, 25.
(29) Lewis, D.; Catlow, C. R. A. *J. Phys. Chem. Solids* **1986**, *47*, 89.
(30) Uchida, S.; Tajima, S.; Masaki, A.; Sugai, S.; Kitazawa, K.; Tanaka, S. *J. Phys. Soc. Jpn.* **1985**, *54*, 4395.

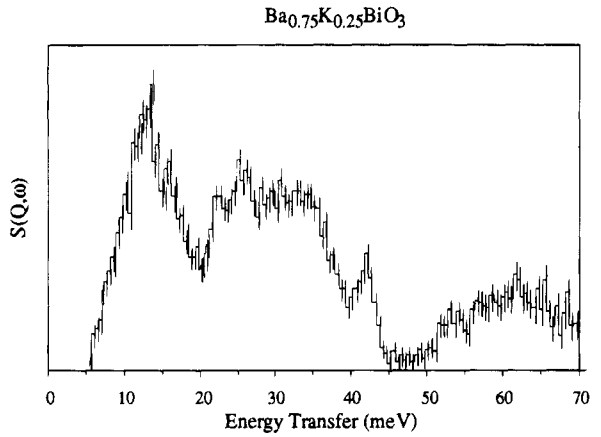

Figure 3. Neutron-weighted phonon density-of-states of $Ba_{0.75}K_{0.25}BiO_3$.

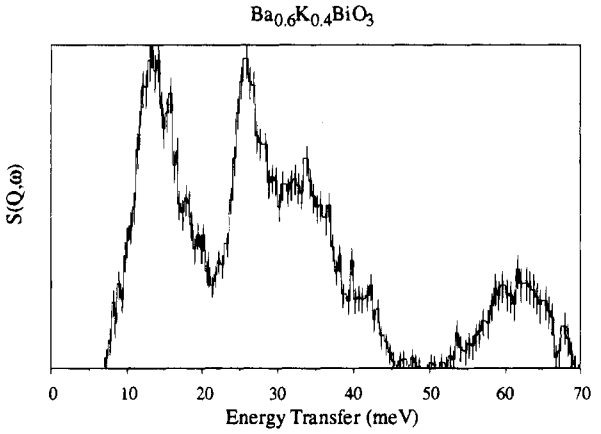

Figure 4. Neutron-weighted phonon density-of-states of $Ba_{0.6}K_{0.4}BiO_3$.

Table 2. Phonon Frequencies and Fwhm's for $Ba_{0.6}K_{0.4}BiO_3$ and $Ba_{0.75}K_{0.25}BiO_3$ at 22 K, Measured on TFXA at 22 K

	$Ba_{0.6}K_{0.4}BiO_3$		$Ba_{0.75}K_{0.25}BiO_3$	
phonon assignment	freq (meV)	fwhm	freq (meV)	fwhm
external TO/acoustic	8.1(3)	3(1)	11.1(2)	5(4)
external TO/acoustic	12.8(2)	4.5(5)	13.2(2)	2(1)
external TO/acoustic	16(1)	13(3)	14.9(8)	15(1)
external TO/acoustic	15.8(4)	0.4(7)	16.1(1)	0.8(2)
external LO	21.9(2)	1.2(4)	22.2(2)	3.6(9)
optically inactive	25.51(6)	4.6(3)	25.7(3)	2.7(6)
bending TO	33.1(3)	13(1)	32.1(3)	15.1(9)
bending LO	42.2(4)	3.8(9)	42.2(1)	2.3(2)
defect	48.2(5)	7(3)	49(1)	6(2)
defect	52.6(3)	3.0(9)	52.4(3)	3(1)
breathing TO	62.0(2)	15.0(7)	61.0(5)	15.0(6)
breathing LO			73.7(5)	6(2)

positions. The TO and LO branches of the optically inactive phonon are calculated to be very close in energy and consequently indistinguishable with powder samples, giving rise to the peak at 25.7 meV. The scattering between 25 and 35 meV is best accounted for by a very broad single peak at 31.1 meV that arises from both the optically inactive phonon and the TO branch of the bending mode, while the feature at 42.3 meV is due to the LO bending mode. Two small features at 49.0 and 52.4 meV are present in the 45–60 meV range; their origin is not immediately apparent since no scattering is predicted by the calculations in this region. Both peaks are strongly sample dependent, and since they do not vary with temperature, we assign them to defect modes. Finally, the broad peak at 61.0 meV and a sharper feature at 73.7 meV are assigned to the TO and LO components of the breathing mode, respectively. Both the octahedral bending and breathing modes, which constitute most of the spectrum above 25 meV, are dominated by oxygen atom vibrations.

Table 2 also shows the results of the Gaussian fit to each of the peaks for superconducting $Ba_{0.6}K_{0.4}BiO_3$. Only minor changes in the spectra are seen on increasing the doping from $x = 0.25$ to $x = 0.4$. The peak at 25.7 meV increases in intensity, confirming its origin as mostly from potassium atoms occupying the perovskite A site. A further consequence of the higher proportion of K is the softening of the modes arising from both the perovskite A and B sites, as a result of substituting a singly charged for a doubly charged ion. The most notable change is the almost complete loss of intensity of the 42 meV mode in the $x = 0.4$ sample compared to $x = 0.25$. The origin of this mode has been extensively debated.[21,31,32] In a single-crystal study of $Ba(Pb,Bi)O_3$, Reichardt et al. found that the phonon mode expected in this region was not experimentally observed; only scattering, without dispersion in Q, was found, that was assigned to a defect mode, arising from a static distortion of the octahedral units.[31] Raman scattering measurements[32] showed this peak developed a Fano line shape at low temperature, indicative of electron–phonon coupling, with important implications for the superconductivity in this system. It was proposed that this peak arises from BiO_n units with $n < 6$. In addition, the intensity and width of this spectral feature is strongly sample dependent and varies with the nature of the dopant ion and its concentration.[21]

To elucidate the composition dependence of the vibrational features of $Ba_{1-x}K_xBiO_3$ in the 38–60 meV region, we measured INS spectra on the BT4 at NIST with the results shown in Figure 5. After normalization of the spectra for sample size and beam exposure, it is clear that the mode at 42 meV distinctly varies with x. It sharpens with increasing x from $x = 0$ to $x = 0.3$, but in the metallic phase at $x = 0.4$, it broadens again with loss of intensity. The phonon calculations in section 3 clearly identify this feature as the LO component of the octahedral bending mode. As shown in Figure 2b for $BaBiO_3$, the lowered symmetry due to the combination of a tilt and a breathing distortion, which doubles the unit cell and the number of phonon modes, leads to the prediction of a more intense, less dispersed mode. However, the reason behind the progressive narrowing in phonon line width from $x = 0$ to 0.3 is not clear. Electron diffraction indicates that there may be an additional incommensurate CDW along [110],[33] for compositions between $0.1 < x < 0.375$, although single-crystal X-ray diffraction failed to confirm the existence of such modulations,[34] which seem to be due to electron beam induced effects.[35,36] It is plausible that the narrowing of the 42 meV mode reflects the progressive

(31) Reichardt, W.; Weber, W. *Jpn. J. Appl. Phys.* **1987**, *26*, 1121.
(32) McCarty, K. F.; Radousky, H. B.; Hinks, D. G.; Zheng, Y.; Mitchell, A. W.; Folkerts, T. J.; Shelton, R. N. *Phys. Rev. B* **1989**, *40*, 2662.
(33) Pei, S.; Zaluzec, N. J.; Jorgensen, J. D.; Dabrowski, B.; Hinks, D. G.; Mitchell, A. W.; Richards, D. R. *Phys. Rev. B* **1989**, *39*, 811.
(34) Wochner, P.; Wang, Q. J.; Moss, S. C.; Sinha, S. K.; Grubel, G.; Chou, H.; Berman, L. E.; Axe, J. D.; Loong, C. K.; Liu, J. Z.; Mosley, W. D.; Klavins, P.; Shelton, R. N. *Phys. Rev. B* **1993**, *47*, 9120.
(35) Hewat, E. A.; Chaillout, C.; Godinho, M.; Gorius, M. F.; Marezio, M. *Physica C* **1989**, *157*, 228.

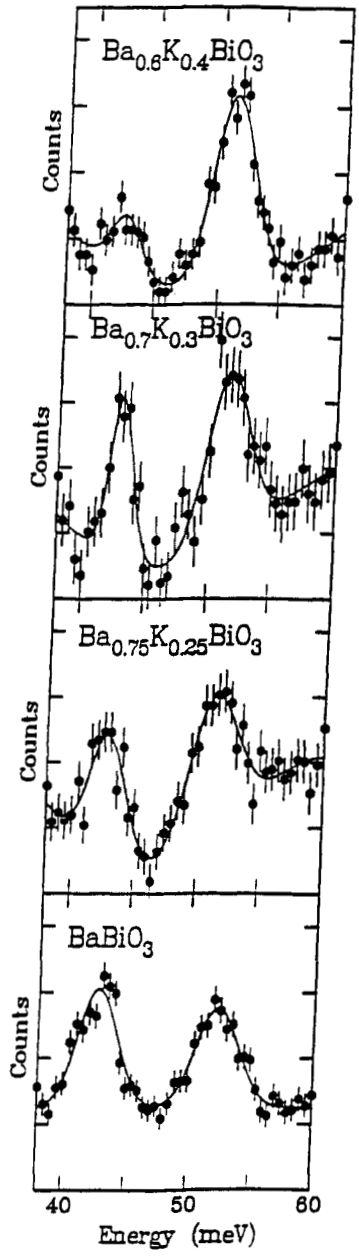

Figure 5. Composition dependence of $Ba_{1-x}K_xBiO_3$ between 35 and 60 meV.

localization of the breathing mode distortion into domains on a length scale $\sim D$, which becomes smaller with increasing x. Dispersion of this defect vibrational mode occurs only for wave vectors Q larger than the inverse coherence length of the distortion, $\sim 1/D$, and as a result, it could lead to a progressive narrowing as the domains shrink in size. Total energy calculations at the local density approximation[35] predict that neither breathing nor tilting distortions are stable alone in $Ba_{1-x}K_xBiO_3$. So, breathing mode distortions, such as those in $BaBiO_3$, are associated with a charge disproportionation, but in this case occur only within these local domains. Local regions of CDW were predicted to be stable in the Ba(Pb,Bi)O_3 system and can readily explain the semiconducting properties in these materials.[37] The local CDW model would also explain the conflicting results from

(36) Verwerft, M.; Van Tendeloo, G.; Hinks, D. G.; Dabrowski, B.; Richards, D. R.; Mitchell, A. W.; Marx, D. T.; Pei, S. Y.; Jorgensen, J. D. *Phys. Rev. B* **1991**, *44*, 9547.
(37) Jurczek, E.; Rice, T. M. *Europhys. Lett.* **1986**, *1*, 225.

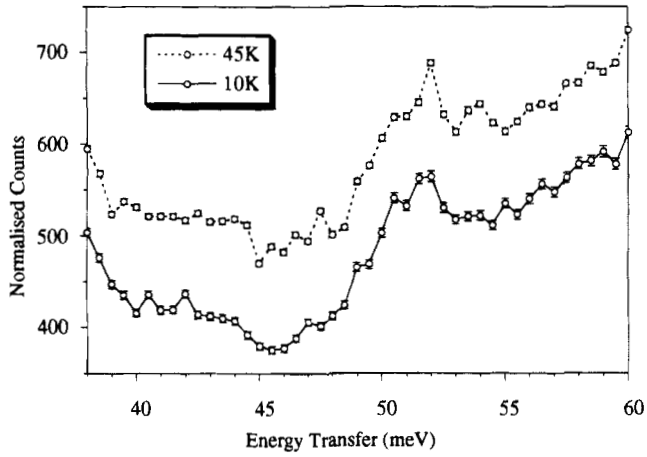

Figure 6. Temperature dependance of $Ba_{0.6}K_{0.4}BiO_3$ over the range 35–60 meV. Measurement performed on the triple-axis spectrometer at NIST.

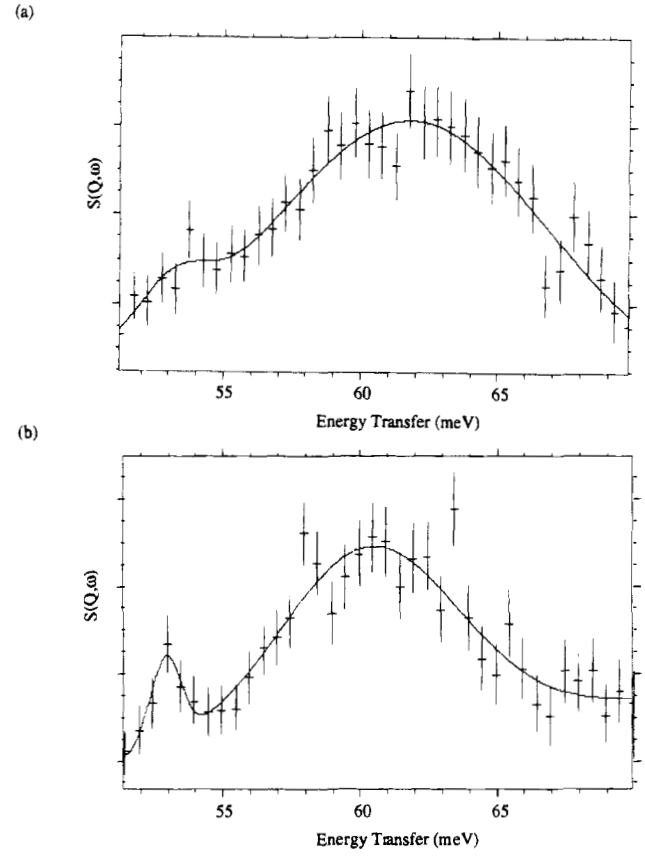

Figure 7. Temperature dependence of the phonon density of states in $Ba_{0.6}K_{0.4}BiO_3$ at (a) 22 K and (b) 45 K.

electron[9,33,34] and X-ray diffraction data,[32] as the wavelength of the incommensurate modulations varies smoothly with increasing K doping and the charge fluctuations are "pinned" by defects caused by the electron beam. These fluctuations would lie outside the neutron or X-ray diffraction time scales, which probe only an average oxygen position but would be manifested in unusual thermal parameters in a Rietveld profile refinement.[9]

Neutron weighted PDOS over the range 35–60 MeV were measured on the triple axis spectrometer at NIST for the superconducting composition $x = 0.4$ above and below T_c at 45 and 10 K (Figure 6). Neither the frequency nor the width of any of the features in the region varies within the error of the experiment. How-

ever, extending these measurements on TFXA over a wider energy range reveals energy shifts and broadenings of both the TO oxygen breathing and bending modes on cooling through the transition temperature at 32 K. Figure 7 shows Gaussian fits to the TO oxygen breathing mode at 45 and 22 K in superconducting $Ba_{0.6}K_{0.4}BiO_3$. Cooling below T_c is accompanied by an increase in the full width at half-maximum, Γ, of the breathing mode from 8.6(6) to 15.0(7) meV and the bending mode from 6(1) to 13(1) meV. On the other hand, the phonon energy shifts exhibit a complicated behavior with the TO bending mode showing a softening from 34.5(2) to 33.1(3) meV and the breathing mode a hardening from 61.1(3) to 62.0(2) meV. This is the first evidence of temperature dependence of the phonon modes above and below T_c in this system. The variations found are broadly consistent with, albeit more pronounced than, those of phonons with frequencies greater than the superconducting energy gap coupling with electrons.[38] This implies that these two modes make the largest contribution to the electron–phonon coupling in the system, which is consistant with tunneling measurements.[19]

Conclusion

The neutron weighted PDOS has been measured for $Ba_{1-x}K_xBiO_3$ as a function of temperature for compositions on either side of the metal–insulator transition at $x \sim 0.375$. Lattice dynamics calculations were employed to aid full assignment of the phonon modes up to 75 meV. Defect modes are identified at ~48 and ~53 meV. The phonon spectra are sensitively affected as the composition varies. In particular, the LO bending mode at ~42 meV is strongly dependent on composition but not on temperature, and we propose that its behavior reflects local structural effects associated with CDW domains of diminishing size as the K doping level increases. However, the frequency, intensity, and line width of the transverse optic (TO) Bi–O breathing (~62 meV) and bending (~33 meV) modes vary significantly as a function of temperature. These anomalies of the TO phonons as a function of temperature are consistent with what is expected for superconductivity via a conventional BCS-like mechanism.

Acknowledgment. We thank the Engineering and Physical Sciences Research Council for financial support and access to ISIS. We also thank the National Institute of Standards and Technology for partial financial support and provision of neutron beam time. We acknowledge helpful discussions with J. J. Rush and J. Tomkinson.

CM940484W

(38) Zeyher, R.; Zwicknagl, G. *Z. Phys. B* **1990**, *78*, 175.